A New DC Charging Station to Control Power Flows on Low Voltage Grids

Dario De Santis

Department of Electrical and Information Engineering, Polytechnic University of Bari, Bari, Italy

Abstract: ***With the development of power electronics and storage systems, the electric vehicles market has grown. So, for this reason low voltage electric grids are experiencing growth in the number of charging stations. There are several power levels to charge an electric vehicle with DC or AC voltage. This paper proposes a double three-phase power supply solution for DC charging stations to charge the vehicle battery and to control active and reactive power flows between two electric feeders using a low voltage UPFC.***

Keywords: Unified Power Flow Controller (UPFC), EV charging station, LV grids, STATCOM converter, SSSC converter

1. Introduction

The EV (Electric Vehicle) has zero emission, it is silent and it has low maintenance costs. Furthermore, thanks to electrical motors (synchronous or induction motor) the EV has better performances than the endothermic engine (diesel or gasoline engine). The only limitation that electric vehicles have, is the electric battery, which reduces the maximal electrical power for electrical motors, reduces the driver range and increases the vehicle cost. On the market, there are electric vehicles with fuel-cells that use hydrogen fuel and/or lithium electric batteries. Nowadays the electric battery system is more convenient, and it is more efficient than the hydrogen system so, on the market this is the main technology for the EV. Thanks to the development of this type of storage, it is possible to reach a good result in terms of performances and the electrical vehicles market is now growing [1]. Hence the charging process and charging devices play a key role for electrical vehicles. On the market, there are two main typologies of charging stations; the AC charging station and the DC charging station [2]. The AC system uses a battery charger on board of the EV. The DC system can be charge the EV battery directly and it is easier to integrate renewable sources. Furthermore, the DC station is more flexible than the AC station for low voltage electric grids, because it is possible to use the AFE converter (Active Front End) to obtain the DC voltage and at the same time to control the reactive power or the voltage level in the PCC (Point of Common Coupling) of the charging station [3]. In this way, it is possible also to charge the EV and to provide ancillary services for the LV (Low Voltage) grid with a V2G (Vehicle to Grid) solution or with an auxiliary battery.

However, in the DC charging station with AFE converter there is no possibility to control active and reactive power flows between the two LV feeders. This aspect is most important in low voltage electrical grids, when a power flow inversion occurs on one of two feeders, due to the distributed generation or when there is an overload problem on one of the two feeders. To solve these issues, it is possible to use a LV-UPFC (Low Voltage Unified Power Flow Controller) to control active and reactive power flows on the interline link [4]. In addition, it is possible to achieve the optimal management of the two feeders to obtain minimal active power losses.

In this paper, the author proposes a new solution for the DC charging station with a double three-phase power supply to charge the EV and at the same time to control the power flow between the two feeders. These feeders are connected to independent low voltage grids, so one feeder is connected to its own transformer and the other is connected to another transformer. This is possible with a SSSC (Static Synchronous Series Compensator) converter with a three-phase series transformer and by an AFE converter in shunt connection. The active front end thus works as a STATCOM (Static Compensator) converter. So, this is the LV-UPFC configuration with a bidirectional DC/DC converter to charge the EV battery [5]. The power scheme of the proposed solution is shown in figure 1. With the SSSC, active and reactive power flows are managed between the two feeders and thanks to the STATCOM, it is possible to manage the active power flow between the EV and the LV grid with a V2G or G2V (Grid to Vehicle) solution. Furthermore, with the shunt converter it is possible to exchange reactive power with the electrical grid in the PCC. The reactive set-point is received from a central distribution system controller or from a voltage controller that it is able to maintain a voltage amplitude value in the PCC. This set-point must be received from a central controller in the same way as a reactive power set-point. The STATCOM converter ensures an active power balance for the SSSC thanks to the voltage control for the DC link capacitor. Therefore, the SSSC works with a PQ control system and the STATCOM works with a $V_{DC}Q$ control or with a $V_{DC}|V_{AC}|$ control [4] [6].

In next paragraph the system overview with main electrical parameters is presented, and then control systems of the STATCOM, SSSC and DC/DC converters are explained using mathematical formulae. Matlab/Simulink software was used to test the control system and the power scheme of the proposed solution. Finally, results in terms of current waveform, active and reactive power are shown in the case of charging the EV and at the same time active and reactive power flows are managed between two feeders by SSSC.

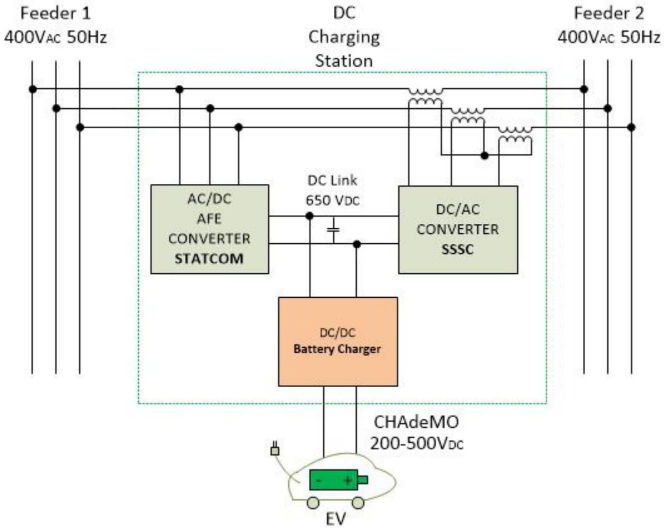

Figure 1: DC Charging station with LV-UPFC configuration

2. System Overview

In the DC charging station proposed, there is an AC/AC conversion system connected between two feeders, with an access to the DC link to charge the EV battery by an integrated DC/DC converter. The AC/AC solution is composed of the STATCOM converter, the SSSC converter and the bi-directional chopper, with IGBT + diode technology [7] where the switching frequency is equal to 10 kHz for all power electronics converters. For AC/DC converters the 2-level configuration has been used.

The STATCOM is connected to the feeder 1 by a L filter with an inductance value equal to 5 mH and with a transformerless solution. In next paragraph, for simplicity, this converter is designated with the letter α. The control system of the STATCOM inverter needs AC current, AC voltage and DC voltage measurements as shown in figure 2 (orange line) to generate PWM signals for IGBTs. Thanks to the STATCOM, it is possible to manage the reactive power or the voltage amplitude in the PCC of the feeder 1 and to assure the power balance between SSSC and DC/DC converters.

The SSSC converter is connected between the feeder 2 and the feeder 1 with a L filter with an inductance value equal to 3 mH and with a series transformer. In next paragraph, for simplicity, this converter is designated with the letter β. The control system of the SSSC inverter needs AC current, AC voltage and DC voltage measurements as shown in figure 2 to generate PWM signals for IGBTs. Thanks to the SSSC, it is possible to manage active and reactive power between the PCC of the feeder 1 and the PCC of the feeder 2, so it is possible to exchange active and reactive power between two independent grids. The active power exchanged between the SSSC and the interline connection is exchanged between the STATCOM and the feeder 1 with inverted flow direction. The DC/DC converter manages the power flow and the current flow between the EV battery and the DC charging station. It is a bidirectional chopper, so it is possible to charge or discharge the battery in G2V or V2G mode. To control the power battery and the current battery dynamic, it is necessary to measure the EV battery voltage, the EV battery current and the DC link voltage.

With the STATCOM $V_{DC}Q$ controller, the active power exchanged with the feeder 1 is given by (1), where P_α is the active power exchanged between the STATCOM and the feeder 1, P_β is the active power exchanged between the SSSC and the interline connection between two feeders, P_{EV} is the EV battery power and P_{loss} is equal to active power losses of the entire system. The load convention for P_α, P_β and P_{EV} has been used; hence the absorbed power is positive.

$$P_\alpha = P_\beta + P_{EV} + P_{loss} \qquad (1)$$

In table 1, the main technical parameters of the DC charging station proposed are shown. The rated power for the EV charging is equal to 20 kW and for the STATCOM is equal to 30 kW with a nominal power factor equal to 1. So, in this way the rated apparent power value is equal to 30 kVA to have the possibility to manage the STATCOM reactive power and the SSSC active power. It is important to note that in the LV-UPFC solution, the SSSC rated active power is less than the STATCOM rated active power because there is not a galvanic decoupling between two feeders, so active and reactive power (between two feeders) are managed by the integrated UPFC in the charging station and flow in the interline link and not in the STATCOM or in the SSSC converter. This means that the SSSC applies a voltage value by a series transformer in relation to the current required to obtain the active and reactive power flows desired between the two feeders. So, the SSSC with the series transformer emulates a serial impedance in the interline link to allow control of the active and reactive power flows.

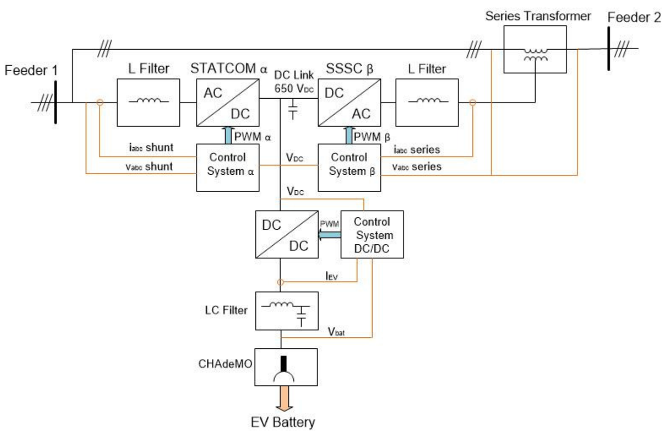

Figure 2: DC Charging station control system overview

Table 1: DC Charging station technical parameters

Parameter	*Value*
Grid 1 rated AC Voltage feeder 1 [V]	400
Grid 2 rated AC Voltage feeder 2 [V]	400
Grids rated frequency [Hz]	50
STATCOM switching frequency [kHz]	10
SSSC switching frequency [kHz]	10
DC/DC switching frequency [kHz]	10
DC link capacitor [μF]	1000
DC link voltage [V]	650
Rated active power [kW]	30
Nominal power factor [p.u.]	1

EV charger rated power [kW]	20
EV battery DC Voltage range [V]	200-500

3. Mathematical Formulation

3.1. STATCOM Converter

Figure 3 shows the plant for the STATCOM converter, where the one phase representation for the positive sequence of the three-phase system is used. The power converter is schematised with a voltage source in accordance with the average model for the VSC (Voltage Source Converter). In the STATCOM scheme, there is an ohmic-inductive impedance for the converter filter, where $L_{f\alpha}$ is the inductive component of the filter and $R_{f\alpha}$ is the ohmic component of the filter. While L_{g1} and R_{g1} are inductive and ohmic components of the Thevenin equivalent model applied in the PCC and e_1 is the voltage of the feeder 1 in no-load condition. The voltage of the power electronics converter is indicated as v_α, it is equal to the average value of PWM phase voltage, and i_α is the converter current.

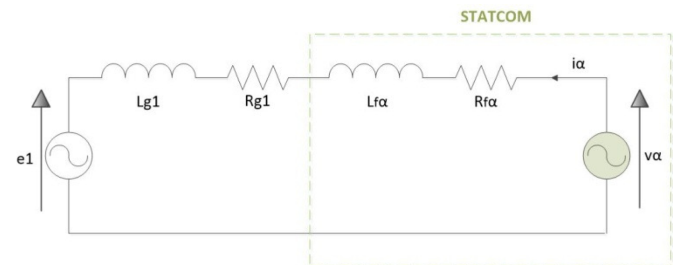

Figure 3: Plant for the STATCOM converter

Applying the Kirchhoff's voltage law to the plant for the STATCOM shown in figure 3, (2) is obtained for the positive sequence. For the three-phase system (4) is used, where $\vec{V}^{\alpha}_{abc}$ is the STATCOM phase voltages' vector, $\vec{I}^{\alpha}_{abc}$ is the line currents' vector and $\overrightarrow{E_1}_{abc}$ is the no load phase voltages' vector of the Thevenin model in the PCC point. The components of these vectors are shown in (3).

$$v_\alpha = \left(R_{f\alpha} + R_{g1}\right) i_\alpha + \left(L_{f\alpha} + L_{g1}\right)\frac{di_\alpha}{dt} + e_1 \quad (2)$$

$$\vec{V}^{\alpha}_{abc} = \begin{vmatrix} v^{\alpha}_a \\ v^{\alpha}_b \\ v^{\alpha}_c \end{vmatrix} \vec{I}^{\alpha}_{abc} = \begin{vmatrix} i^{\alpha}_a \\ i^{\alpha}_b \\ i^{\alpha}_c \end{vmatrix} \overrightarrow{E_1}_{abc} = \begin{vmatrix} e_{1a} \\ e_{1b} \\ e_{1c} \end{vmatrix} \quad (3)$$

$$\vec{V}^{\alpha}_{abc} = \left(R_{f\alpha} + R_{g1}\right)\vec{I}^{\alpha}_{abc} + \left(L_{f\alpha} + L_{g1}\right)\frac{d\vec{I}^{\alpha}_{abc}}{dt} + \overrightarrow{E_1}_{abc} \quad (4)$$

To obtain direct and quadrature components in the rotating frame, the Park matrix T shown in (5) is used, with the angle of the synchronous rotating frame ϑ_{dq} calculated by PLL [8] using the VOC technique (Voltage Orientated Control) [9].

$$\mathrm{T} = \frac{2}{3}\begin{pmatrix} \cos(\vartheta_{dq}) & \cos\left(\vartheta_{dq} - \frac{2}{3}\pi\right) & \cos\left(\vartheta_{dq} + \frac{2}{3}\pi\right) \\ -\sin(\vartheta_{dq}) & -\sin\left(\vartheta_{dq} - \frac{2}{3}\pi\right) & -\sin\left(\vartheta_{dq} + \frac{2}{3}\pi\right) \\ \frac{1}{2} & \frac{1}{2} & \frac{1}{2} \end{pmatrix} \quad (5)$$

The direct and the inverse Park transformation is expressed by (6) for currents and voltages to obtain direct, quadrature and homopolar components and vice versa.

$$\begin{vmatrix} x_d \\ x_q \\ x_0 \end{vmatrix} = T \begin{vmatrix} x_a \\ x_b \\ x_c \end{vmatrix} \quad \begin{vmatrix} x_a \\ x_b \\ x_c \end{vmatrix} = T^{-1} \begin{vmatrix} x_d \\ x_q \\ x_0 \end{vmatrix} \quad (6)$$

In this work, the homopolar component is neglected for currents and voltages, for the STATCOM and for the SSSC because these converters work in balanced conditions. (7) is obtained thanks to (6), where $\vec{V}^{\alpha}_{dq}$ is the STATCOM phase voltages' vector in dq frame, $\vec{I}^{\alpha}_{dq}$ is the line currents' vector in dq frame and $\overrightarrow{E_1}_{dq}$ is the no load phase voltages' vector in dq frame. Using R_α equal to the total resistance of the plant and L_α equal to the total inductance of the plant by (8), the plant equation (9) is obtained applying the Kirchhoff's voltage law in the rotating frame. Thanks to (9) the PI current controller for direct and quadrature components has been designed.

$$\vec{V}^{\alpha}_{dq} = \begin{vmatrix} v^{\alpha}_d \\ v^{\alpha}_q \end{vmatrix} \vec{I}^{\alpha}_{dq} = \begin{vmatrix} i^{\alpha}_d \\ i^{\alpha}_q \end{vmatrix} \overrightarrow{E_1}_{dq} = \begin{vmatrix} e_{1d} \\ e_{1q} \end{vmatrix} \quad (7)$$

$$R_\alpha = R_{f\alpha} + R_{g1} \; L_\alpha = L_{f\alpha} + L_{g1} \quad (8)$$

$$\vec{V}^{\alpha}_{dq} = R_\alpha \vec{I}^{\alpha}_{dq} + L_\alpha \frac{d\vec{I}^{\alpha}_{dq}}{dt} + j\omega_{dq} L_\alpha \overrightarrow{I^{\alpha}_{dq}} + \overrightarrow{E_1}_{dq} \quad (9)$$

To obtain the direct current reference $i^{\alpha^*}_d$ (10) is used, where V^*_{DC} is the set-point for the DC link voltage, V_{DC} is the DC link voltage measured and $K^{V_{DC}}_p$ and $K^{V_{DC}}_i$ are respectively the proportional gain and the integrator gain of the voltage PI controller. To obtain the quadrature current reference $i^{\alpha^*}_q$ (11) is used where Q^{α^*} is the reactive set-point received from the central controller. Thanks to (10) it is possible to obtain (1) at steady state.

$$i^{\alpha^*}_d = K^{V_{DC}}_p\left(V^*_{DC} - V_{DC}\right) + K^{V_{DC}}_i \int \left(V^*_{DC} - V_{DC}\right) dt \quad (10)$$

$$i^{\alpha^*}_q = -\frac{Q^{\alpha^*}}{\frac{3}{2} e_{1d}} \quad (11)$$

In (12), $\vec{I}^{e\alpha}_{dq}$ is equal to the currents' error vector in the rotating frame and Ω^α is the de-coupling matrix. The pulsation ω_{dq} is calculated by PLL. Then with (13) is defined the $C^{I\alpha}_p$ matrix for proportional gains of the currents' loop PI and $C^{I\alpha}_i$ matrix for integrator gains of the currents' loop PI. Finally, in (14) the matrix equation to implement the currents' controller for direct and quadrature components is shown (U is the identity matrix). The outputs of this controller are STATCOM phase voltages in the rotating frame. These voltages are used to obtain PWM gate signals to send to the IGBTs of the PWM converter [10].

$$\vec{I}^{e\alpha}_{dq} = \begin{vmatrix} i^{\alpha^*}_d - i^{\alpha}_d \\ i^{\alpha^*}_q - i^{\alpha}_q \end{vmatrix} \Omega^\alpha = \begin{pmatrix} 0 & -\omega_{dq} L_\alpha \\ \omega_{dq} L_\alpha & 0 \end{pmatrix} \quad (12)$$

$$C^{I\alpha}_p = \begin{pmatrix} K^{I\alpha}_p & 0 \\ 0 & K^{I\alpha}_p \end{pmatrix} C^{I\alpha}_i = \begin{pmatrix} K^{I\alpha}_i & 0 \\ 0 & K^{I\alpha}_i \end{pmatrix} \quad (13)$$

$$\vec{V}^{\alpha}_{dq} = C^{I\alpha}_p \vec{I}^{e\alpha}_{dq} + C^{I\alpha}_i \int \vec{I}^{e\alpha}_{dq} dt + \Omega^\alpha \vec{I}^{\alpha}_{dq} + U\overrightarrow{E_1}_{dq} \quad (14)$$

Paper ID: ART20173045 DOI: 10.21275/ART20173045

International Journal of Science and Research (IJSR)
ISSN (Online): 2319-7064
Index Copernicus Value (2015): 78.96 | Impact Factor (2015): 6.391

Figure 4 shows the STATCOM control system schematic representation with V_{DC}/Q controller and direct and inverse Park transformations for line currents and phase voltages.

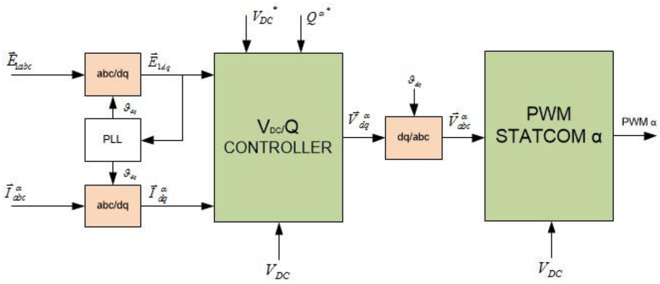

Figure 4: STATCOM Control system

The STATCOM V_{DC}/Q controller is shown in figure 5, where schematic representations for (10) and (11) and the schematic representation for (14) are shown.

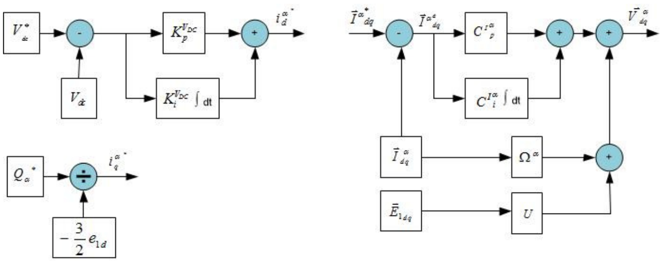

Figure 5: STATCOM Control loops

STATCOM control parameters are listed in table 2, where the proportional gain and the integrator gain for the inner currents' control loop and for the V_{DC} voltage's control loop are shown with L_α and R_α values.

Table 2: STATCOM Control parameters

Parameter	*Value*
Current controller proportional gain Kp [V/A]	20.00
Current controller integrator gain Ki [V/A]	666.67
Total inductance Lα [mH]	6.00
Total resistance Rα [Ω]	0.20
DC Voltage controller proportional gain Kp [A/V]	2.00
DC Voltage controller integrator gain Ki [A/V]	6.67

3.2. SSSC Converter

In figure 6 the plant for the SSSC converter is shown, where the one phase representation for the positive sequence of the three-phase system is used. The power converter is schematised with a voltage source in accordance with the average model for the VSC. In the SSSC scheme, there is an ohmic-inductive impedance for the converter filter, where $L_{f\beta}$ is the inductive component of the filter and $R_{f\beta}$ is the ohmic component of the filter. The quantity v1 is the voltage of the feeder 1 and v2 is the voltage of the feeder 2. The output voltage of the power electronics converter is indicated as v_β. It is equal to the average value of PWM phase voltage and i_β is the current converter.

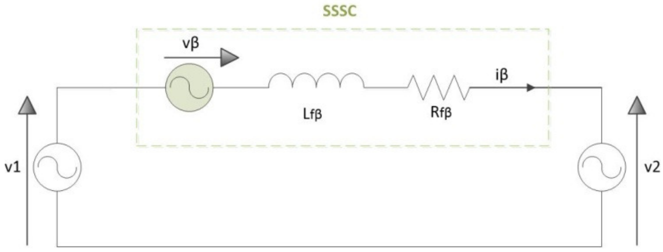

Figure 6: Plant for the SSSC converter

Applying the Kirchhoff's voltage law to the plant for the SSSC shown in figure 6, (15) for the positive sequence is obtained. For the three-phase system (17) is used, where $\vec{V}^{\beta}_{abc}$ is the SSSC phase voltages' vector, $\vec{I}^{\beta}_{abc}$ is the converter currents' vector, $\vec{V_1}_{abc}$ is the phase voltages of the feeder 1 vector and $\vec{V_2}_{abc}$ is the phase voltages of the feeder 2 vector. The components of these vectors are shown in (16).

$$v_\beta = R_{f\beta} i_\beta + L_{f\beta}\frac{di_\beta}{dt} + v_2 - v_1 \quad (15)$$

$$\vec{V}^{\beta}_{abc} = \begin{vmatrix} v^{\beta}_a \\ v^{\beta}_b \\ v^{\beta}_c \end{vmatrix} \vec{I}^{\beta}_{abc} = \begin{vmatrix} i^{\beta}_a \\ i^{\beta}_b \\ i^{\beta}_c \end{vmatrix} \vec{V_1}_{abc} = \begin{vmatrix} v_{1a} \\ v_{1b} \\ v_{1c} \end{vmatrix} \vec{V_2}_{abc} = \begin{vmatrix} v_{2a} \\ v_{2b} \\ v_{2c} \end{vmatrix} \quad (16)$$

$$\vec{V}^{\beta}_{abc} = R_{f\beta}\vec{I}^{\beta}_{abc} + L_{f\beta}\frac{d\vec{I}^{\beta}_{abc}}{dt} + \vec{V_2}_{abc} - \vec{V_1}_{abc} \quad (17)$$

To obtain direct and quadrature components in the rotating frame the Park matrix T (5) is used, with the angle ϑ_{dq} equal to the STATCOM synchronous rotating frame angle. (18) is obtained applying (6), where $\vec{V}^{\beta}_{dq}$ is the SSSC phase voltages' vector in dq frame, $\vec{I}^{\beta}_{dq}$ is the converter currents' vector in dq frame, $\vec{V}_{1dq}$ is the phase voltages of the feeder 1 vector in dq frame and $\vec{V}_{2dq}$ is the phase voltages of the feeder 2 vector in dq frame. (19) is obtained applying the Kirchhoff's voltage law in the rotating frame. Thanks to (19) the PI current controller for direct and quadrature components has been designed.

$$\vec{V}^{\beta}_{dq} = \begin{vmatrix} v^{\beta}_d \\ v^{\beta}_q \end{vmatrix} \vec{I}^{\beta}_{dq} = \begin{vmatrix} i^{\beta}_d \\ i^{\beta}_q \end{vmatrix} \vec{V_1}_{dq} = \begin{vmatrix} v_{1d} \\ v_{1q} \end{vmatrix} \vec{V_2}_{dq} = \begin{vmatrix} v_{2d} \\ v_{2q} \end{vmatrix} \quad (18)$$

$$\vec{V}^{\beta}_{dq} = R_\beta \vec{I}^{\beta}_{dq} + L_\beta \frac{d\vec{I}^{\beta}_{dq}}{dt} + j\omega_{dq} L_\beta \overrightarrow{I^{\beta}_{dq}} + \vec{V_2}_{dq} - \vec{V_1}_{dq} \quad (19)$$

To obtain the direct current reference $i^{\beta^*}_d$ and the quadrature current reference $i^{\beta^*}_q$ (20) is used, where P* is the set-point of the active power between two feeders and Q* is the set-point of the reactive power between two feeders.

$$\begin{vmatrix} i^{\beta^*}_d \\ i^{\beta^*}_q \end{vmatrix} = \frac{2}{3}\frac{1}{{v_1}_d^2 + {v_1}_q^2}\begin{pmatrix} v_{1d} & v_{1q} \\ v_{1q} & -v_{1d} \end{pmatrix}\begin{vmatrix} P^* \\ Q^* \end{vmatrix} \quad (20)$$

In (21), $\vec{I}^{e\beta}_{dq}$ is equal to the currents' error vector in the rotating frame and Ω^β is the de-coupling matrix. The pulsation ω_{dq} is calculated by PLL and it is equal to the STATCOM control pulsation. Then with (22) is defined the $C^{I\beta}_p$ matrix for proportional gains of the currents' loop PI and $C^{I\beta}_i$ matrix for integrator gains of the currents' loop PI.

Finally, in (23) the matrix equation to implement the currents' controller for direct and quadrature components is shown (U is the identity matrix). The outputs of this controller are SSSC phase voltages in the rotating frame. These voltages are used to obtain PWM gate signals to send to the IGBTs of the PWM converter.

$$\vec{I}_{dq}^{e\beta} = \begin{vmatrix} i_d^{\beta *} - i_d^{\beta} \\ i_q^{\beta *} - i_q^{\beta} \end{vmatrix} \Omega^{\beta} = \begin{pmatrix} 0 & -\omega_{dq} L_{\beta} \\ \omega_{dq} L_{\beta} & 0 \end{pmatrix} \quad (21)$$

$$C_p^{I\beta} = \begin{pmatrix} K_p^{I\beta} & 0 \\ 0 & K_p^{I\beta} \end{pmatrix} C_i^{I\beta} = \begin{pmatrix} K_i^{I\beta} & 0 \\ 0 & K_i^{I\beta} \end{pmatrix} \quad (22)$$

$$\vec{V}_{dq}^{\beta} = C_p^{I\beta} \vec{I}_{dq}^{e\beta} + C_i^{I\beta} \int \vec{I}_{dq}^{e\beta} dt + \Omega^{\beta} \vec{I}_{dq}^{\beta} + U(\vec{V_2}_{dq} - \vec{V_1}_{dq}) \quad (23)$$

Figure 7 shows the SSSC control system schematic representation with the P/Q controller and direct and inverse Park transformations for line currents and phase voltages for both feeders.

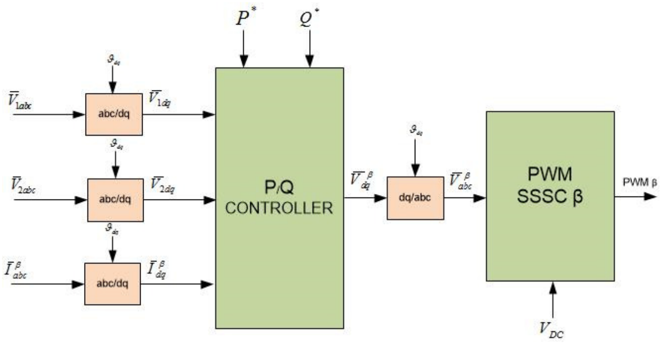

Figure 7: SSSC Control system

The SSSC P/Q controller is shown in figure 8, where the schematic representation for (20) and (23) is shown.

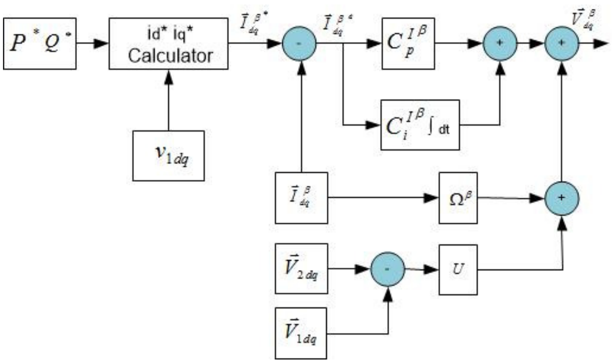

Figure 8: SSSC Control loops

SSSC control parameters are listed in table 3, where the proportional gain and the integrator gain for the inner currents' control loop are shown with L_β and R_β values.

Table 3: SSSC Control parameters

Parameter	*Value*
Current controller proportional gain Kp [V/A]	10.00
Current controller integrator gain Ki [V/A]	333.33
Inductance L_β [mH]	3.00
Resistance R_β [Ω]	0.10

3.3. DC/DC Converter

In figure 9, the plant for the DC/DC converter is shown, where the electric car battery is represented by Thevenin model. E_{bat} is equal to no load condition voltage and R_{bat} is the resistance to represent the power losses in the battery and in the connection cables between the EV and the DC charging station. The DC/DC power converter is schematised with a DC voltage source with an ohmic-inductive-capacitive impedance for the converter filter, where L_f is the inductive component of the filter, R_f is the ohmic component of the filter and C_f is the filter capacitor. V_{EV} is the DC/DC average voltage output applied to the LC filter and it is obtained from the EV power control. In table 4, the plant parameters are summarised.

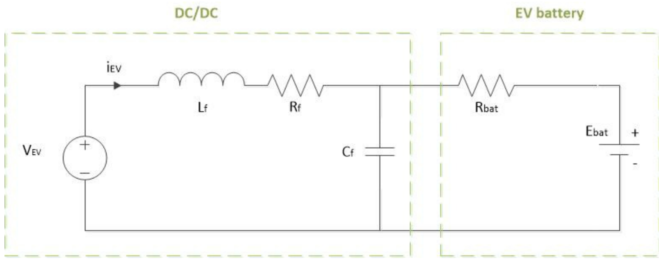

Figure 9: Plant for the DC/DC converter

Table 4: DC/DC Plant parameters

Parameter	*Value*
Battery voltage E_{bat} [V]	300
Battery resistance R_{bat} [Ω]	0.3
DC/DC output filter inductance L_f [mH]	5
DC/DC output filter resistance R_f [Ω]	0.1
DC/DC output filter capacitor C_f [μF]	50

Applying the Kirchhoff's voltage law to the EV plant shown in figure 9, (24) is obtained. For simplicity, the capacitor effect has been neglected, because this component does not influence the design of the current's controller for the EV battery. The capacitor is used only to obtain a little ripple in the output voltage.

$$V_{EV} = (R_f + R_{bat}) i_{EV} + L_f \frac{di_{EV}}{dt} + E_{bat} \quad (24)$$

The DC/DC control has two loops: the outer loop to control the bi-directional power to charge/discharge the EV battery and the inner loop to control the EV battery current dynamic. So, to obtain the reference for the current's control loop (26) is used, where i_{EV}^* is the current reference for the inner loop, K_p^{PEV} is the proportional gain of the power PI controller and K_i^{PEV} is the integrator gain of the power PI controller. The power error is equal to e_P^{EV} and it is calculated with (25), where P_{EV}^* is the power set-point for the EV battery from the central control system and P_{EV} is the instantaneous EV battery power measured.

$$e_P^{EV} = P_{EV}^* - P_{EV} \quad (25)$$

$$i_{EV}^* = K_p^{PEV} e_P^{EV} + K_i^{PEV} \int e_P^{EV} dt \quad (26)$$

So, thanks to (27) the current error for the current PI is obtained, where i_{EV} is the instantaneous EV battery current measured.

With (28) the modulation index m is obtained for PWM, where K_p^{IEV} and K_i^{IEV} is the proportional gain and the integrator gain respectively for the PI current's controller. Finally, the output voltage V_{EV} is given by (29).

$$e_I^{EV} = i_{EV}^* - i_{EV} \tag{27}$$

$$m = K_p^{IEV} e_I^{EV} + K_i^{IEV} \int e_I^{EV} dt + \frac{E_{bat}}{V_{DC}} \tag{28}$$

$$V_{EV} = mV_{DC} \tag{29}$$

In figure 10 the scheme of the DC/DC control system is shown, where the power controller receives the power set-point P_{EV}^* from the central control and thanks to EV voltage battery and EV current battery measurements, it is able to set the modulation index m to obtain PWM signals to send to the IGBTs of the bidirectional chopper.

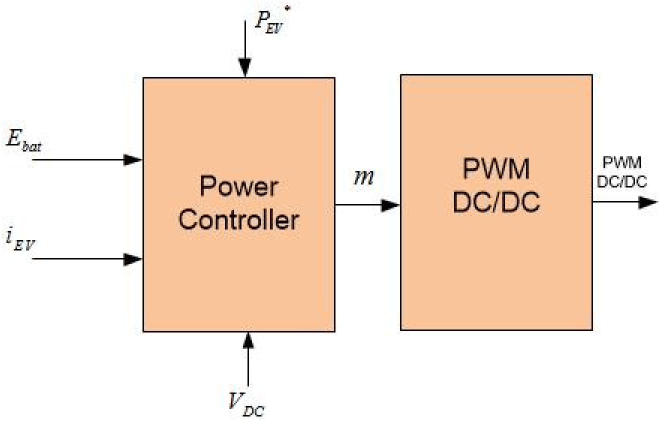

Figure10: DC/DC Control system

The DC/DC power controller is shown in figure 11, where the schematic representation for (26) and (28) is shown.

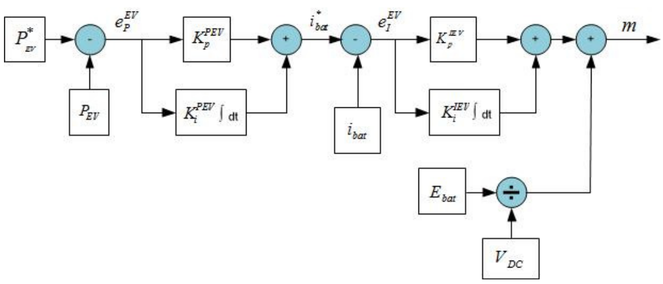

Figure 11: DC/DC Control loops

DC/DC control parameters are summarised in table 5, where the proportional gain and the integrator gain for the inner current's control loop are shown, and table 5 lists the proportional gain and the integrator gain for the power's control loop.

Table 5: DC/DC Control parameters

Parameter	*Value*
Current controller proportional gain Kp [p.u./A]	0.01
Current controller integrator gain Ki [p.u./A]	1
Power controller proportional gain Kp [A/W]	0.001
Power controller integrator gain Ki [A/W]	0.1

4. Simulation Results

To test the DC charging station, two study cases have been considered. In the first one, there is a simulation of a congestion emergency in the grid 2 where the DC charging station charges the EV with 10 kW and there are two loads, one for each feeder; the DC charging station is able to supply the load in the grid 2 avoiding the protection intervention. In the second case the DC charging station charges the EV with 5 kW and in the grid 2 there is an inversion of the power flow due to the solar generation, so to use the excess power, the DC charging station charges the EV with 15 kW using 10 kW from the grid 2 and 5 kW from the grid 1.

4.1. Case 1

In this case, the DC charging station charges the EV with 10 kW and the grid 1 supplies in initial condition the EV and the load 1 with 5 kW and 2 kVAr. Instead grid 2 supplies the load 2 with 10 kW and 5 kVAr, and active and reactive power flows between two feeders are equal to zero. A congestion emergency occurs at 0.3 s where the grid 2 is not able to supply the load 2, and so thanks to the device proposed, it is possible to supply the load 2 using the grid 1. Thus it is possible to avoid the protection intervention and to assure the normal service in the grid 2. In figure 12, the power scheme used is shown and in table 6, the case 1 technical parameters are summarised.

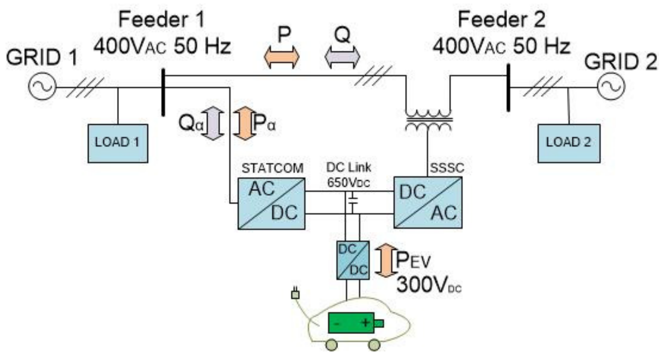

Figure 12: Scheme to test the DC charging station Case 1

Table 6: Case 1 parameters

Parameter	*Value*
Load 1 active power [kW]	5
Load 1 reactive power [kVAr]	2
Load 2 active power [kW]	10
Load 2 reactive power [kVAr]	5
EV charge power [kW]	10
EV battery voltage [V]	300

In figure 13 all active and reactive power of the system are shown. The EV battery power is equal to 10 kW for all simulation time, and it is kept constant thanks to the DC/DC control system. The grid 1 supplies the load 1 in initial condition and the EV, thanks to the STATCOM converter, with the active power equal to 15 kW and the reactive power equal to 2 kVAr. The STATCOM works with a power factor equal to 1. The grid 2 supplies only the load 2 in initial condition, with the active power equal to 10 kW and the reactive power equal to 5 kVAr. At time equals 0.3 s, the SSSC converter thanks to the interline series link, to avoid the contingence emergency in grid 2, exchanges active and reactive power between the feeder 1 and the feeder 2, so now, the grid 1 supplies the load 1, the load 2 and the EV battery with 25 kW as active power and 7 kVAr as reactive power, while as shown in figure 13 active and reactive power supplied by grid 2 are equal to zero.

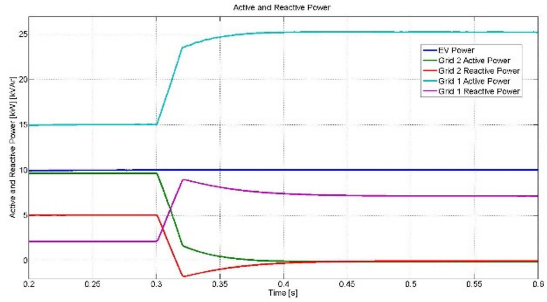

Figure 13: Active and Reactive Power Case 1

In figure 14, the PCC voltages of the feeder 1 are shown and figure 15 shows the PCC voltages of the feeder 2. It is possible to see a small decrease in PCC voltages in the feeder 1 at time equals 0.3 s due to the increment of active and reactive power supplied by grid 1, while in the PCC of the feeder 2 it is possible to see a small increase in voltage amplitudes at time equals 0.3 s due to the decrement of active and reactive power supplied by grid 2.

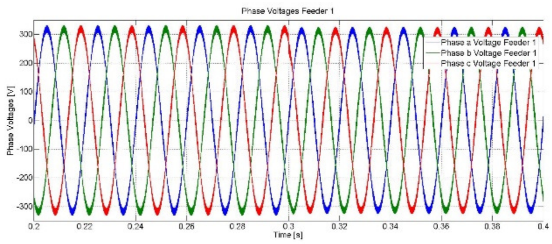

Figure 14: PCC Phase Voltages Feeder 1 Case 1

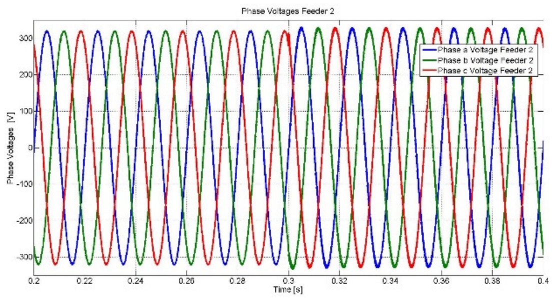

Figure 15: PCC Phase Voltages Feeder 2 Case 1

In figure 16, line currents of the grid 1 are shown and figure 17 shows line currents of the grid 2. It is possible to see the increment of line currents of the grid 1 at time equals 0.3 s due to the increment of active and reactive power supplied by grid 1, while in the grid 2 it is possible to see the decrement of line currents at time equals 0.3 s, due to the decrement of active and reactive power supplied by grid 2. Furthermore, in figure 18, interline currents between two feeders are shown, where before the time equals 0.3 s interline currents are equal to zero, after time equals 0.3 s thanks to SSSC, interline currents are not zero and they depend on active and reactive power exchanged between two feeders. Finally, in figure 19, the EV battery voltage and the EV battery current are shown.

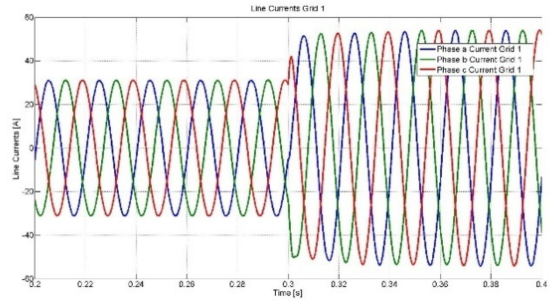

Figure 16: Line Currents Grid 1 Case1

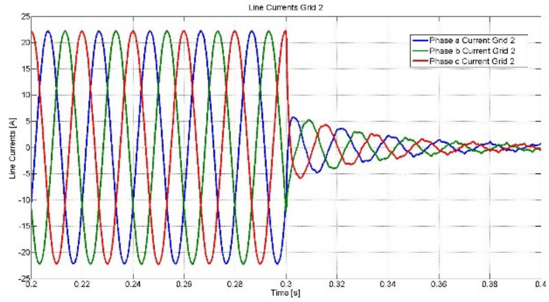

Figure 17: Line Currents Grid 2 Case 1

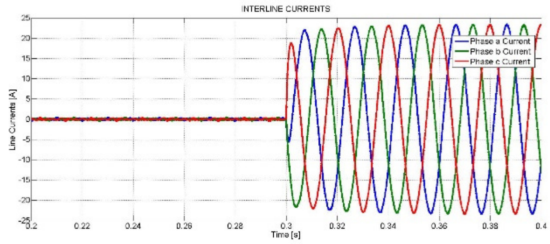

Figure 18: Interline Currents Case 1

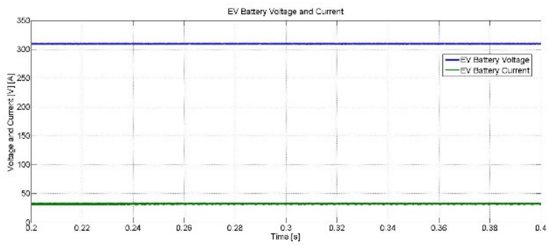

Figure 19: EV Battery Voltage and Current Case 1

4.2. Case 2

In this case, in initial condition the DC charging station charges the EV with 5 kW and the grid 1 supplies the load 1 with 5 kW and 2 kVAr. Instead the grid 2 receives the active power from the solar inverter with a power flow inversion equal to 10 kW. To use green power in a better way, and to avoid the flow inversion on the grid 2, the SSSC is used to exchange the active power flow between two feeders at time equals 0.3 s, in such way that green power is used to supply EV avoiding the flow inversion and reducing the charge cost. So, the EV charge power is increased to 15 kW to use green power. In figure 20, the power scheme used is shown and in table 7, the case 2 technical parameters are summarised.

International Journal of Science and Research (IJSR)
ISSN (Online): 2319-7064
Index Copernicus Value (2015): 78.96 | Impact Factor (2015): 6.391

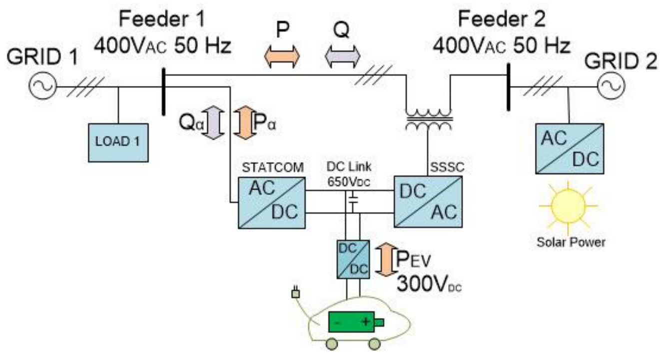

Figure 20: Scheme to test the DC charging station Case 2

Table 7: Case 2 parameters

Parameter	*Value*
Load 1 active power [kW]	5
Load 1 reactive power [kVAr]	2
Solar inverter output power [kW]	10
EV charge power (using SSSC) [kW]	15
EV battery voltage [V]	300

Figure 21 shows all active and reactive power of the system. The EV battery charge power is equal to 5 kW, when the power is supplied only by grid 1 and it is equal to 15 kW when, thanks to the SSSC, the EV battery is supplied by both feeders at time equals 0.3 s; 5 kW from the grid 1 and 10 kW from the solar generator connected on the feeder 2. The grid 1 in initial condition supplies the load 1 and the EV thanks to the STATCOM converter, with the active power equal to 10 kW and the reactive power equal to 2 kVAr. In the grid 2 there is a power flow inversion in initial condition with the active power equal to -10 kW due to the solar generator and in this case, there are not any loads. At time equals 0.3 s, the SSSC converter, thanks to the interline series link, to avoid the active power flow inversion in the grid 2 and to use green solar power in the better way, exchanges only the active power between the feeder 1 and the feeder 2, so the grid 1 supplies the load 1 and the EV battery with 10 kW as active power and 2 kVAr as reactive power (same values before SSSC operation), while as shown in figure 21, active and reactive power supplied by grid 2 are equal to zero. In this way thanks to the DC charging station proposed in this paper, the active power flow inversion in the grid 2 has been avoided and green solar power has been used to optimise the charge time of the EV.

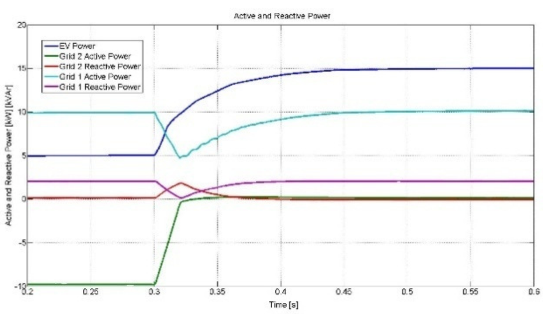

Figure 21: Active and Reactive Power Case 2

In figure 22 PCC voltages of the feeder 1 are shown and figure 23 shows the PCC voltages of the feeder 2. In this case both phase voltage amplitudes are practically constant for the whole simulation time. In figure 24, the line currents of the grid 1 are shown and in figure 25, the line currents of the grid 2 are shown. It is interesting to see that the currents in the grid 1 do not change at steady state because the grid 1 supplies the same active and reactive power. But in the transient time, at 0.3 s, the currents decrease because the active power dynamic by SSSC from the feeder 2 is faster than the EV battery power dynamic that increases from 5 kW to 15 kW. Instead, in the grid 2 it is possible to see the decrement of line currents at time equals 0.3 s due to the SSSC operation that moves green solar power towards the feeder 1 to charge the EV. Furthermore, in figure 26 interline currents between two feeders are shown, where before the time equals 0.3 s, interline currents are equal to zero, but after time equals 0.3 s interline currents are not zero and they depend on the active power exchanged. Finally, in figure 27 the EV battery voltage and the EV battery current are shown; it is possible to see the increment of voltage and current at time equals 0.3 s to use green solar power.

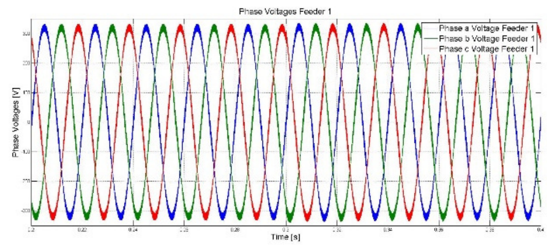

Figure 22: PCC Phase Voltages Feeder 1 Case2

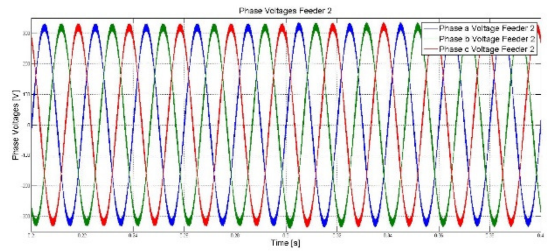

Figure 23: PCC Phase Voltages Feeder 2 Case2

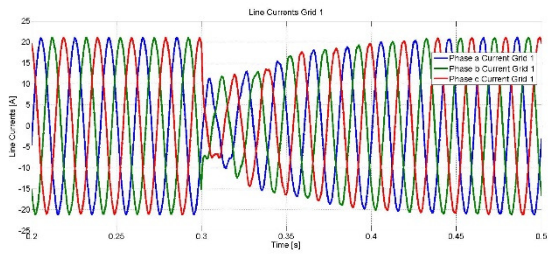

Figure 24: Line Currents Grid 1 Case2

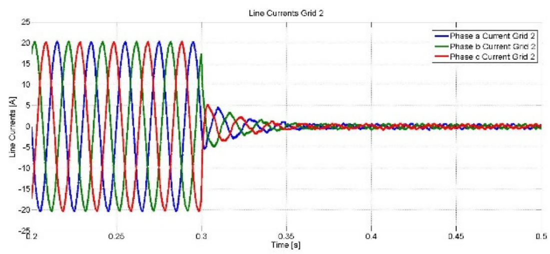

Figure 25: Line Currents Grid 2 Case2

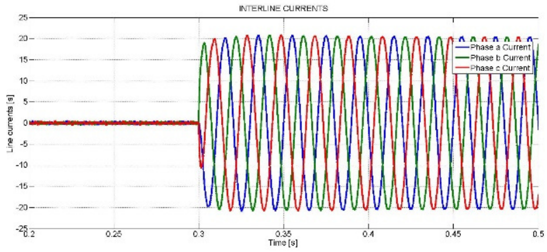

Figure 26: Interline Currents Case2

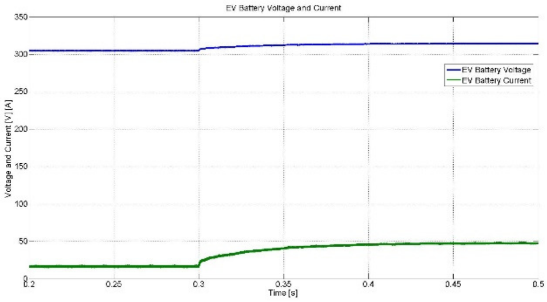

Figure 27: EV Battery Voltage and Current Case 2

5. Conclusion

This paper proposes a new DC charging station, where thanks to the SSSC converter, it is possible to obtain a low voltage UPFC integrated in an all-in-one solution. In this way, it is possible to charge or discharge the EV in G2V or V2G mode and it is possible to control the reactive power or the voltage level in the PCC thanks to the STATCOM converter. But with the SSSC converter, it is possible also to exchange active and reactive power between two feeders to solve some typical problems in LV grids. With Matlab/Simulink, STATCOM, SSSC and DC/DC converters have been modelled and two study cases have been simulated to test SSSC converter operations during the EV battery charging and to see the effects on low voltage distribution grids. Simulation results confirm the mathematical formulation validity for all operations. In the future, it will be possible to build this device and to install it in some grids with an active power flow inversion or with congestion problems in one of the two feeders.

References

[1] A. G. Boulanger, A. C. Chu, S. Maxx and D. L. Waltz, “Vehicle Electrification: Status and Issues,” Proceedings of the IEEE, vol. 99, pp. 1116-1138, May 2011.

[2] M. Yilmaz and P. T. Krein, “Review of Battery Charger Topologies, Charging Power Levels, and Infrastructure for Plug-In Electric and Hybrid Vehicles,” IEEE Transactions on Power Electronics, vol.28, pp. 2151-2169, Aug 2012.

[3] D. De Santis, G. Abbatantuono, S. Bruno and M. La Scala, “Low Voltage Grid Control through Electrical Vehicles Charging Stations,” WSEAS Transactions on Power Systems, vol. 11, pp. 283-288, 2016.

[4] D. De Santis, G. Abbatantuono, S. Bruno, M. La Scala and R. Sbrizzai,“ Control of Power Flows in Low Voltage Distribution Systems,” WSEAS Transactions on Power Systems, vol. 11, pp. 276-282, 2016.

[5] K. M. Tan, V. K. Ramachandaramurthy and J. Y. Yong, “Bidirectional Battery Charger for Electric Vehicle,” IEEE Innovative Smart Grid Technologies - Asia (ISGT Asia), May 2014.

[6] D. G. Cho and E. H. Song, “A simple UPFC control algorithm and simulation on stationary reference frame,” IEEE International Symposium on Industrial Electronics ISIE 2001, June 2001.

[7] N. Iwamuro and T. Laska, "IGBT History, State-of-the-Art, and Future Prospects," IEEE Transactions on Electron Devices, vol.64, pp. 741-752, Feb 2017.

[8] B. Meersman, J. De Kooning, T. Vandoorn, L. Degroote, B. Renders and L. Vandevelde, “Overview of PLL methods for Distributed Generation units,” Universities Power Engineering Conference (UPEC), 2010 45th International, Sept 2010.

[9] T. Zhao, Q. Zong, T. Zhang and Y. Xu, “Study of Photovoltaic Three-Phase Grid-Connected Inverter Based on the Grid Voltage-Oriented Control,” IEEE 11th Conference on Industrial Electronics and Applications (ICIEA), Jun 2016.

[10] F. Blaabjerg, R. Teodorescu, M. Liserre and A. V. Timbus, “Overview of Control and Grid Synchronization for Distributed Power Generation Systems,” IEEE Transactions on Industrial Electronics, vol. 53, pp.1398-1409, Oct 2006.

Author Profile

Dario De Santis received his B.Sc. and M.Sc. degrees in Electrical Engineering from the Polytechnic University of Bari in 2011 and 2014 respectively. Now he is a licensed Senior Electrical Engineer and he is pursuing a Ph.D. degree in Electrical Engineering. His research interests include power electronics for low voltage electrical grids, electrical mobility and smart metering systems for grid automation.